Geochemical evolution of groundwater in a basaltic aquifer based on chemical and stable isotopic data: Case study from the Northeastern portion of Serra Geral Aquifer, São Paulo state (Brazil)

Didier Gastmans [a,*], Ian Hutcheon [b], Amauri Antônio Menegário [a,1], Hung Kiang Chang [c,2]

[a] Centro de Estudos Ambientais, UNESP – Univ Estadual Paulista, Av. 24A, 1515 Bela Vista, Rio Claro, SP CEP: 13506-900, Brazil
[b] Department of Geoscience, Applied Geochemistry Group, University of Calgary, 2500 University Drive NW, Calgary, Alberta T2N 1N4, Canada
[c] Centro de Estudos Ambientais and Laboratório de Estudos de Bacias, UNESP – Univ Estadual Paulista, Av. 24A, 1515 Bela Vista, Rio Claro, SP CEP: 13506-900, Brazil

A R T I C L E   I N F O

S U M M A R Y

Groundwater from the fractured basalt Serra Geral Aquifer (SGA) represents an important source for water supply in Northeastern São Paulo state (Brazil). Groundwater flow conditions in fractured aquifers hosted in basaltic rocks are difficult to define because flow occurs through rock discontinuities. The evaluation of hydrodynamic information associated with hydrochemical data has identified geochemical processes related to groundwater evolution, observed in regional flowpaths. SGA groundwaters are characterized by low TDS with pH varying from neutral to alkaline. Two main hydrochemical facies are recognized: Ca–Mg–HCO$_3$, and Na–HCO$_3$ types. Primarily, the geochemical evolution of SGA groundwater occurs under CO$_2$ open conditions, and the continuous uptake of CO$_2$ is responsible for mineral dissolution, producing bicarbonate as the main anion, and calcium and magnesium in groundwater. Ion exchange between smectites (Na and Ca-beidelites) seems to be responsible for the occurrence of Na–HCO$_3$ groundwater. Toward the Rio Grande, in the northern portion of the study area, there is mixing between SGA groundwater and water from the sandstones of the Guarani Aquifer System, as evidenced by the chemical and isotopic composition of the groundwater. Inverse mass balance modeling performed using NETPATH XL produces results in agreement with the dissolution of minerals in basalt (feldspars and pyroxenes) associated with the uptake of atmospheric CO$_2$, as well as the dissolution of clay minerals present in the soil. Kaolinite precipitation occurs due to the incongruent dissolution of feldspars, while Si remains almost constant due to the precipitation of silica. The continuous uptake of CO$_2$ under open conditions leads to calcite precipitation, which in addition to ion exchange are responsible by Ca removal from groundwater and an increase in Na concentrations. Down the flow gradient CO$_2$ is subject to closed conditions where the basalts are covered by the sediments of Bauru Group or associated with deeper isolated discontinuities. A decrease in the amount of dissolution of labradorite and augite is observed, associated with precipitation of carbonates and kaolinite. Stable isotope ratios of SGA groundwater vary from −37.8‰ to −61.3‰ VSMOW for δ^{2}H VSMOW, and −5.7‰ to −8.9‰ VSMOW for δ^{18}O, indicating temporal variations in climatic conditions during recharge.

1. Introduction

Basaltic rock aquifers represent an important groundwater resource, hosting water supply in several parts of the world.

Basalts are good aquifers because they store water of excellent quality, generally characterized by low salinity, and the thickness and spatial extension of basaltic lava flows provide high storage capacity. Basaltic lava flows typically have geologic discontinuities responsible for groundwater storage and flow in these units (Deolankar, 1980; Léonardi et al., 1996; Domenico and Schwartz, 1998; Bourlier et al., 2005; Dafny et al., 2003, 2006; Lastoria et al., 2006; among others). Basaltic provinces around the world constitute excellent aquifer units including: Deccan Plateau in India (Deolankar, 1980; Kulkarni et al., 2000), Columbia River Plateau in USA (Deutsch et al., 1982), Golan Heights in Israel (Dafny

et al., 2006), and the Atherton Tabelands in North Queensland, Australia (Locsey and Cox, 2003), among others.

Evaluation of groundwater hydrochemistry and isotopic composition is being increasingly used to complement studies focused on understanding the flow condition and origin of groundwater in fractured and heterogeneous aquifers units, such as basaltic aquifers. Hydrochemistry can be an aid to define chemical reactions produced by water–rock interaction and stable isotope data ($\delta^{18}O$ and $\delta^{2}H$) can be used as tracer of groundwater origin, mixing of waters of different origins, as well as to interpret paleoclimate recharge conditions for groundwater (Aggarwal et al., 2005). Combining these analytical data allows the construction of geochemical models, which can be used to determine the evolution of groundwater along flow paths in aquifers, based on the interpreted reactions and processes related to water–rock interactions or anthropogenic sources (Plummer et al., 1990; Rosenthal et al., 1998; Bouhlassa and Aiachi, 2002; Bretzler et al., 2011; among others).

Located in the Southeastern portion of South America, the Paraná Sedimentary Basin is comprised of a vulcano-sedimentary sequence up to 8000 m thick, with a generally elliptical shape that has the major axis trending NE–SW. Among several sedimentary units, the Serra Geral Aquifer (SGA) is an important Cretaceous volcanic stratigraphic unit that can reach up to 1500 m thick in the center of the sedimentary basin, and is one of the most important aquifers located in the region (Fig. 1). The SGA represents an important water source for public supply, irrigation and industrial purposes, largely in the states of Paraná, Santa Catarina, Rio Grande do Sul and Mato Grosso do Sul, Brazil, as well as in Argentina, Paraguay and Uruguay. Hydrochemical studies of groundwater in the SGA have been conducted in the southern portion of Brazil, allowing groundwater chemical characterization and the establishment of the hydraulic relationship with the underlying unit, the Guarani Aquifer (Bittencourt, 1996; Bittencourt et al., 2003; Boff et al., 2006; Buchmann Filho et al., 2002; Lastoria, 2002; Lastoria et al., 2006; Machado et al., 2002; Nanni, 2008, among others). Aquifers in Mesozoic rocks of the Paraná Sedimentary Basin (Bauru, Serra Geral and Guarani Aquifers) provide public water supply in the West portion of São Paulo state. Due to the importance of these units in the region, the hydrodynamics and hydrochemistry of the Guarani and Bauru aquifers have been studied since the 1970s, and several conceptual models for groundwater flow and hydrochemical evolution have been formulated (eg. Gallo and Sinelli, 1980; da Silva, 1983; Kimmelmann e Silva et al., 1986; Rebouças, 1994; Campos, 1987, 1993; Meng and Maynard, 2001; Sracek and Hirata, 2002; Barison, 2003; Paula e Silva et al., 2005; Gastmans et al., 2010; among others). However, the hydrochemical and hydrogeological characteristics of the SGA have not been studied extensively.

This study has three main objectives. First, to recognize and characterize the water types that exist in the basaltic aquifer, based on their chemical composition. Second, to examine the geochemical evolution and stable isotope composition of SGA groundwater along selected flow paths, thereby defining a set of possible reactions based on changes in groundwater composition and related to the observed mineralogy of the aquifer. Based on these possible reactions, using NETPATH XL (Plummer et al., 1994; Parkhurst and Charlton, 2008), mass transfer along a number of flow paths is tested, as well as the possibility of mixing with groundwater from the underlying unit (Guarani Aquifer System). The third objective is to evaluate the isotopic data to determine the effect of variations in climatic conditions over SGA groundwater stable isotope ratios.

2. Geological and hydrogeological settings

Basalts of the Serra Geral Formation are present in the Paraná Magmatic Province (PMP), which constitutes one of the largest volcanic manifestations of basic rocks in a continental area. This magmatic province includes lava flows and intrusive basic rocks (sills and dykes) representing, according to Milani et al. (1994), an important contribution to generation of continental crust during the Mesozoic. The radiometric ages indicate that volcanic activity began between 133 and 132 Ma, starting in the South and moved towards the North in a relatively short interval of approximately 3 Ma (Renne et al., 1992, 1996; Ernesto et al., 1999). This vast volume of basaltic lavas reaches thicknesses up to 2000 m toward the center of the Paraná Sedimentary Basin, and was deposited over the aeolian sandstones of the Botucatu Formation, which constitutes one of the stratigraphic units of the Guarani Aquifer System.

The greatest part of the magmatic volume of the Serra Geral Formation (up to 97%) is represented by basalts and andesites, while in the southern region of Brazil rhyodacites and rhyolites (Palmas (ATP) and rhyodacites and quartz latitites Chapecó (ATC)) are recognized (Bellieni et al., 1986; Nardy et al., 2002). In São Paulo state there are mainly basalts of mafic to intermediate composition, consisting of plagioclase (mainly labradorite), pyroxene (augite and piegonite), and olivine, mainly as pseudomorphs (Machado et al., 2007). Vesicular zones of variable thickness are recognized at the boundary between basaltic lava flow events. Secondary minerals forming amygdales fill these vesicles, including quartz, calcite, zeolites, fluorite and commonly greenish clays, probably of the celadonite group (Machado, 2007). The occurrence of mordenite and other minerals of the zeolite group has been described by Shinzato et al. (2008) and Frank (2008). The intense weathering of basaltic rocks is responsible for the very deep soils observed in the southern portion of Brazil, and the weathering of plagioclase produces gibbsite and amorphous silica, while pyroxenes weather to smectite, goethite, and gibbsite (Clemente and Azevedo, 2007).

Rebouças and Fraga (1988) present a generic hydrogeological model for groundwater flow conditions in the basalts of the Serra Geral Formation. They recognize permeable and impermeable zones for each lava flow event. At the top and bottom of each sequence, a highly permeable zone is observed, associated with basalt weathering, and groundwater flow is associated with the occurrence of a vesicular basaltic layer that has extensive horizontal fractures. The central portion of each sequence represents an aquitard, where minor vertical movement of water is associated with vertical discontinuities (joints and fractures). A groundwater flow conceptual model for the basaltic aquifer in the region of Ribeirão Preto (SP-BR), including possible recharge toward the underlying unit, the Guarani Aquifer, was proposed by Wahnfried (2010) and Fernandes et al. (2010). They suggested groundwater flow predominantly along horizontal discontinuities in the basaltic rocks and a lack of vertical flow through the geological lineaments, identified by aerial surveys, that limits recharge of the underlying Guarani Aquifer by water from the Serra Geral basalts.

Groundwater flow in the study area for the SGA is driven by the topography, with flow from elevated areas, located in the East, westward towards the main rivers that cross the basalt outcrop areas (Fig. 2). This suggests that the SGA in the study area is an unconfined aquifer, at least in the outcrop zone, and the main rivers represent local discharge zones. Gastmans and Chang (2012) recognized the existence of an artesian zone in the Guarani Aquifer along the rivers Pardo, Sapucaí, Mogi Mirim and Grande, and some groundwater contribution coming from groundwater flow from the underlying Guarani Aquifer toward basaltic discontinuities might be expected, leading to the potential for mixing with SGA.

Groundwater from the SGA has low electrical conductivities (EC), due to low total dissolved solids (TDS), and a wide range of pH values, from acid to alkaline. The chemical composition shows the groundwater to be mainly Ca–HCO_3 and Ca–Mg–HCO_3 type (DAEE, 1974, 1976; Campos, 1993). In the Northwestern region
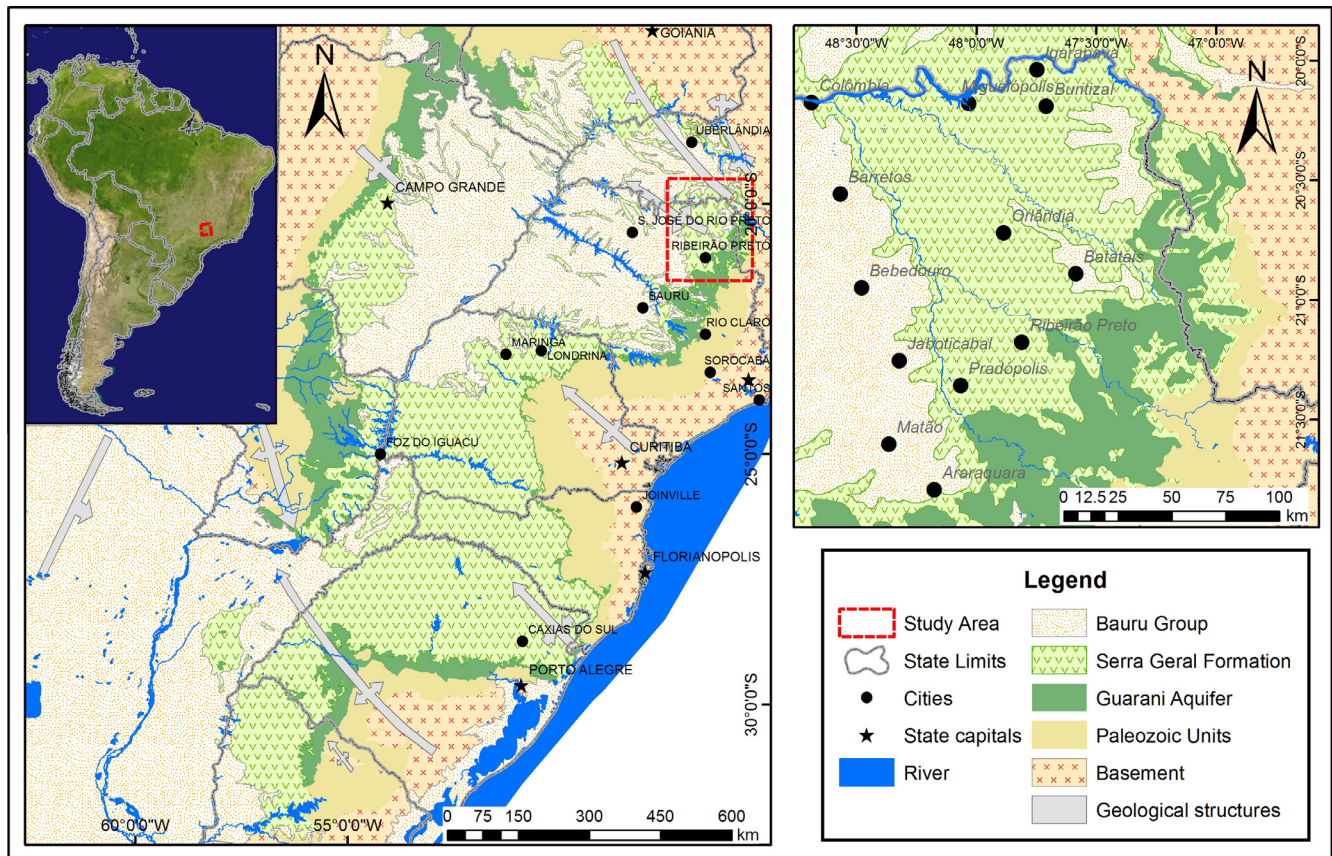
Fig. 1. Location map of the Serra Geral Aquifer, showing in detail the study area (Regional geological base map modified from OEA, 2009 – left map, and local geological base map modified from DAEE/UNESP (1980)).

of São Paulo state hydrochemical anomalies have been recognized, characterized by TDS values up to 200 mg L^{-1}, and associated with fractures or faults filled by hydrothermal mineralization. These anomalies may be due to contamination by more saline waters originating from underlying aquifers (DAEE, 1976).

3. Methods

Thirty-one groundwater samples were collected directly from water supply wells. The location of sampled wells, drilled in basalts of the SGA, is presented in Fig. 2. The pH, electrical conductivity, dissolved oxygen and temperature of each water sample was measured in the field. The sample was filtered (0.45 μm) and part was acidified using HNO$_3$ to pH < 2 for cation analysis and part preserved refrigerated (approximately 4 °C) for anion analysis. Results of field measured data and chemical analysis are presented in Table 1.

The cation and anion concentrations in groundwater samples were determined in the Hydrogeology and Hydrogeochemistry Laboratory of the Department of Applied Geology IGCE/UNESP Rio Claro. Alkalinity was determined by titration, while anions (F$^-$, Cl$^-$, NO$_3^-$, PO$_4^{2-}$ and SO$_4^{2-}$) were measured by ion chromatography and cations (Na$^+$, K$^+$, Ca^{2+}, Mg^{2+}, Al^{3+} and Si) were measured by ICP-AES. The quality of water analyses was checked by charge balance ($\Delta_{meq} = 100 \cdot (\Sigma^+_{meq} - \Sigma^-_{meq})/(\Sigma^+_{meq} + \Sigma^-_{meq}) < 10\%$). Only sample ASG-SP-108 shows a difference of 11%, acceptable for the purpose of this work. Twenty-four samples collected for the determination of water isotopic content (δ^{18}O and δ^2H) were stored in 200 mL polyethylene bottles, and in order to prevent isotope

fractionation, the excessive presence of air inside the bottle were avoided. Stable isotope ratios (δ^{18}O and δ^2H) were analyzed in the Environmental Isotope Laboratory at the Department of Earth and Environmental Sciences at the University of Waterloo-CAN, by Laser Absorption Spectroscopy. These results, reported as ‰ relative to Vienna Standard Mean Ocean Water (VSMOW) are presented in Table 2.

The geochemical computer program PHREEQC (Parkhurst and Appelo, 1999) was used to calculate saturation indices, PCO$_2$, activities of dissolved species in the groundwater and estimate the Al concentrations in samples presenting concentrations below the limit of detection, by considering groundwaters to be in equilibrium with kaolinite. All calculations were performed at the temperature measured in the field. If the temperature was not measured, calculations were accomplished at 25 °C, which is considered the average temperature in the aquifer.

A weighted average of eleven rainwater events sampled in Rio Claro during 2013 (SP, location in Fig. 1, and composition in Table 1), was used as the initial water composition for inverse mass balance modeling. Rain samples were collected using a simple rain gauge installed on the UNESP Campus, and procedures for sample preservation and analysis are the same described for groundwater samples.

Controls over groundwater chemistry, especially variations of Ca^{2+} and Na$^+$ concentrations, based on equilibrium-exchange reactions were investigated by constructing activity–activity diagrams. Geochemist's Workbench (Bethke, 2007) was used to construct the diagram, considering primary and secondary minerals observed in the Serra Geral basalts. Minerals considered include kaolinite, gibbsite, anorthite, albite, smectite and laumontite. The silica
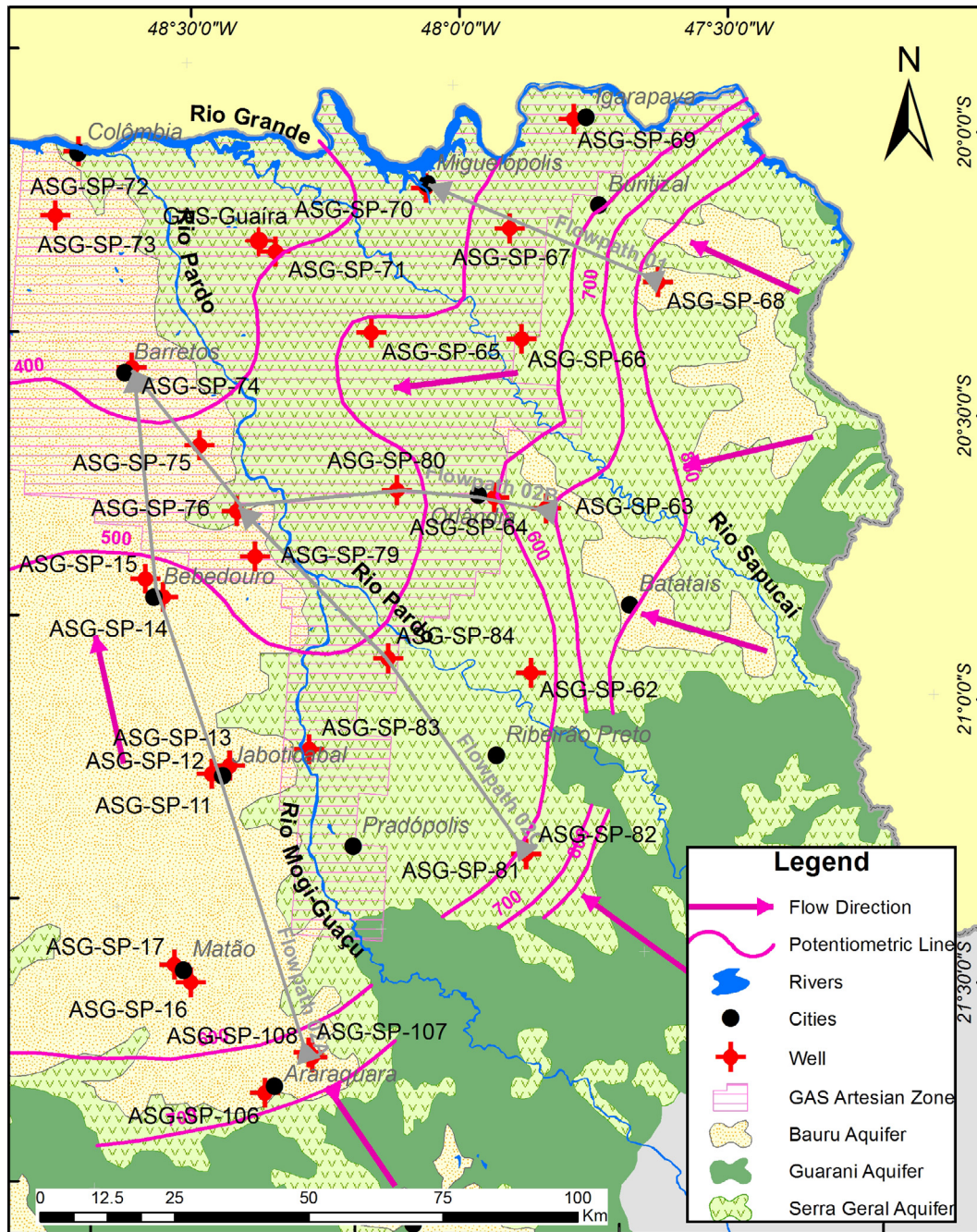
Fig. 2. Location map of sampled wells, showing the simplified groundwater potentiometric map for SGA in the study area, based on water level information from well reports archived in DAEE (Dep. Águas e Energia Elétrica do Estado de São Paulo). Selected flow paths for geochemical mass balance model using NETPAHT XL code (Plummer et al., 1994; Parkhurst and Charlton, 2008) are indicated in the map (Geological base map modified from DAEE/UNESP (1980)).

activity was set by equilibrium with amorphous silica, and the temperature is 25 °C and pressure is 1.0 bar. To evaluate the chemical evolution of groundwater in SGA from rainwater recharge to higher TDS waters, geochemical processes proposed to occur were tested for plausibility along hypothetical flow paths using the modeling code NETPATH XL (Plummer et al., 1994; Parkhurst and Charlton, 2008). NETPATH XL suggests possible reactions on the basis of constraints (dissolved elements) and phases (minerals which are present and dissolved and/or precipitate), using inverse modeling techniques to construct geochemical reactions models. NETPATH XL produces geochemical mass balance reactions between an initial and final water composition. There are no thermodynamic constraints in the code, and thus results of speciation

modeling with PHREEQC (Table 2), and available mineralogical evidence were used to choose possible phases. The purpose of this simulation was to test possible geochemical reactions along the flow path against know water chemistry using a simple mass balance model. NETPATH XL was chosen (new version of NETPATH, Parkhurst and Charlton, 2008) which uses Microsoft Excel® for data entry replacing the data-handling functions of NETPATH.

Geochemical reactions considered were based on the dissolution of minerals observed in the Serra Geral Formation basalts and clay and carbonate minerals recognized as alteration, or in overlying soils. Clay minerals present in the soil may facilitate Ca/Na and Mg/Na exchange, therefore exchange processes were also considered. Weathering introduces CO_2, and incongruent

Table 1
Hydrochemical data set (concentrations in mmol L^{-1}).

Sample	Locality	EC (µS cm^{-1})	pH	DO (mg L^{-1})	Temp. (°C)	HCO$_3$	CO$_3$	Total Alk. (as HCO$_3$)	Cl$^-$	NO$_3^-$	SO$_4^{2-}$	F$^-$	Na	K	Ca	Mg	Al	Si	TDS	Mass balance (%)
ASG-SP-11	Jaboticabal	157.1	7.8	6.90	24.0	1.596	0.000	1.597	0.002	<0.001	<0.0002	0.004	0.207	0.182	0.462	0.190	<0.00002	0.997	3.640	2.70
ASG-SP-12	Jaboticabal	62.9	5.7	6.31	24.7	0.080	0.000	0.080	0.131	0.269	0.002	0.001	0.088	0.167	0.076	0.051	0.0004	0.252	1.116	2.34
ASG-SP-13	Jaboticabal	50.0	7.5	4.00	24.6	0.431	0.000	0.431	0.003	0.026	<0.0002	0.003	0.070	0.174	0.077	0.045	<0.00002	0.456	1.286	2.63
ASG-SP-14	Bebedouro	156.4	8.5	5.24	26.2	1.604	0.151	1.642	0.001	0.004	0.001	0.005	1.322	0.042	0.183	0.006	<0.00002	0.577	3.783	1.47
ASG-SP-15	Bebedouro	298.0	9.6	0.51	27.6	0.942	2.293	1.497	0.293	<0.001	0.267	0.036	3.110	0.008	0.029	0.001	<0.00002	0.933	6.175	3.69
ASG-SP-16	Matão	370.0	9.9	nm	26.7	1.573	4.059	2.556	0.014	<0.001	0.031	0.024	4.006	0.009	0.021	0.005	<0.00002	0.605	7.272	4.69
ASG-SP-17	Matão	272.0	7.4	3.68	27.9	2.185	0.000	2.185	0.168	0.429	0.005	0.005	0.397	0.094	0.916	0.311	<0.00002	0.616	5.126	2.58
ASG-SP-62	Jardinópolis	83.6	7.7	7.11	26.8	0.829	0.000	0.830	0.001	<0.001	0.001	0.006	0.088	0.249	0.213	0.086	<0.00002	0.321	1.795	5.36
ASG-SP-63	Nuporanga	92.6	7.3	4.23	24.6	0.803	0.000	0.803	0.074	0.093	<0.0002	0.005	0.103	0.103	0.312	0.132	<0.00002	0.534	2.159	5.77
ASG-SP-64	Orlândia	109.2	7.2	5.78	24.2	1.029	0.000	1.030	0.018	0.097	0.001	0.004	0.274	0.043	0.339	0.139	<0.00002	0.634	2.578	5.08
ASG-SP-65	Ipuã	55.0	7.1	7.16	25.3	0.493	0.000	0.493	0.012	0.044	0.002	0.011	0.234	0.007	0.149	0.047	<0.00002	0.534	1.533	5.81
ASG-SP-66	Guará	96.4	7.2	3.46	28.0	0.724	0.000	0.725	0.060	0.181	0.001	0.003	0.592	0.017	0.145	0.062	<0.00002	0.360	2.144	2.60
ASG-SP-67	Ituverava	158.8	7.9	nm	28.1	1.688	0.000	1.689	0.011	0.018	0.004	0.005	1.392	0.029	0.125	0.070	<0.00002	0.456	3.798	2.19
ASG-SP-68	Jeriquara	95.7	7.5	3.08	23.9	1.008	0.000	1.008	0.002	0.004	0.001	0.004	0.129	0.058	0.352	0.130	<0.00002	0.694	2.381	6.08
ASG-SP-69	Igarapava	27.2	6.9	5.44	25.3	0.162	0.000	0.162	0.015	0.073	<0.0002	0.002	0.055	0.013	0.064	0.047	<0.00002	0.329	0.760	6.91
ASG-SP-70	Miguelópolis	245.0	9.4	2.87	27.6	1.852	1.546	2.227	0.018	0.023	0.025	0.016	2.827	0.012	0.041	0.017	0.0010	0.431	5.636	3.95
ASG-SP-71	Guaíra	259.0	9.6	nm	24.8	1.575	2.100	2.083	0.054	0.100	0.007	0.008	3.106	0.007	0.023	0.001	0.0030	0.442	5.832	6.01
ASG-SP-72	Colômbia	194.9	7.3	4.17	26.8	1.254	0.000	1.254	0.252	0.463	0.002	0.004	0.439	0.031	0.569	0.289	<0.00002	1.054	4.449	5.02
ASG-SP-73	Colômbia	122.1	7.8	4.07	25.0	1.147	0.000	1.148	0.033	0.108	0.001	0.005	0.148	0.062	0.417	0.191	<0.00002	0.815	2.927	4.77
ASG-SP-74	Barretos	186.4	8.7	1.74	26.4	1.901	0.319	1.979	0.001	0.006	0.010	0.009	1.696	0.052	0.162	0.050	<0.00002	0.709	4.675	1.76
ASG-SP-75	Jaborandi	95.2	7.7	nm	nm	0.993	0.000	0.993	0.018	0.019	0.003	0.004	0.223	0.041	0.274	0.180	<0.00002	0.819	2.575	5.96
ASG-SP-76	Terra Roxa	203.0	8.1	nm	nm	1.852	0.000	1.852	0.123	0.177	0.004	0.008	0.835	0.020	0.571	0.166	<0.00002	0.748	4.506	3.60
ASG-SP-79	Viradouro	51.4	7.1	4.64	27.2	0.426	0.000	0.426	0.032	0.038	0.003	0.005	0.328	0.004	0.069	0.042	0.0003	0.337	1.284	4.26
ASG-SP-80	Morro Agudo	136.5	8.1	nm	30.9	1.480	0.000	1.480	0.002	<0.001	0.002	0.005	0.444	0.059	0.487	0.084	<0.00002	0.268	2.831	4.84
ASG-SP-81	Cravinhos	115.7	7.6	nm	23.9	1.060	0.000	1.061	0.048	0.120	0.001	0.004	0.151	0.048	0.372	0.205	<0.00002	0.726	2.735	4.62
ASG-SP-82	Cravinhos	85.7	7.3	nm	23.5	0.726	0.000	0.726	0.039	0.106	0.002	0.002	0.113	0.038	0.247	0.172	<0.00002	0.588	2.032	5.85
ASG-SP-83	Barrinha	122.4	7.9	6.40	29.0	1.319	0.000	1.320	0.004	0.003	0.002	0.005	0.158	0.054	0.566	0.078	<0.00002	0.320	2.509	5.90
ASG-SP-84	Pontal	181.5	7.9	4.25	29.2	1.852	0.000	1.852	0.029	0.039	0.006	0.001	0.449	0.027	0.843	0.025	<0.00002	0.381	3.652	6.77
ASG-SP-106	Araraquara	192.0	7.9	nm	nm	1.375	0.000	1.375	0.072	0.166	0.022	0.021	0.375	0.070	0.536	0.221	<0.00002	0.741	3.599	7.71
ASG-SP-107	Am. Brasiliense	133.8	7.5	nm	nm	1.232	0.000	1.233	0.049	0.096	0.002	0.005	0.124	0.112	0.417	0.299	<0.00002	0.837	3.173	9.18
ASG-SP-108	Am. Brasiliense	95.8	7.0	nm	nm	0.888	0.000	0.889	0.019	0.075	<0.0002	0.003	0.091	0.044	0.257	0.296	<0.00002	0.698	2.372	11.44
Guaíra – GAS[a]	Guaíra	257.0	9.3	nm	34.7	1.596	0.000	1.597	0.080	0.010	0.069	0.004	2.871	0.006	0.059	0.015	0.0007	0.353	5.064	1.33
Rain	Rio Claro	8.6	5.8	nm	nm	0.080	0.000	0.080	0.008	0.018	0.007	0.006	0.006	0.005	0.018	0.005	<0.00002	<0.002	0.153	3.50

nm – not measured.
[a] Extracted from Reis (2011).

Table 2
Stable isotopes data and thermodynamic Calculations.

Sample	Locality	$\delta^{18}O$ (‰ VSMOW)	δ^2H (‰ VSMOW)	SI quartz	SI Chalc	SI SiO₂(aq)	SI calcite	SI dolomite	P_{CO2}	Al[b] (mmol L^{-1})
ASG-SP-11	Jaboticabal	−7.31	−45.13	0.99	0.56	−0.29	−0.33	−0.92	−2.82	6.64E−06
ASG-SP-12	Jaboticabal	nm	nm	0.39	−0.04	−0.88	−4.44	−8.93	−1.99	nd
ASG-SP-13	Jaboticabal	nm	nm	0.64	0.21	−0.63	−1.90	−3.91	−3.07	nd
ASG-SP-14	Bebedouro	−7.22	−46.89	0.70	0.28	−0.56	−0.01	−1.33	−3.51	8.04E−05
ASG-SP-15	Bebedouro	−7.48	−52.83	0.69	0.27	−0.57	−0.12	−1.47	−4.95	nd
ASG-SP-16	Matão	−8.79	−59.55	0.37	−0.05	−0.89	0.10	−0.22	−5.08	nd
ASG-SP-17	Matão	−6.48	−42.51	0.73	0.31	−0.52	−0.28	−1.13	−2.27	7.52E−06
ASG-SP-62	Jardinópolis	−6.88	−43.17	0.46	0.03	−0.80	−0.97	−2.19	−2.98	nd
ASG-SP-63	Nuporanga	−6.65	−44.12	0.71	0.28	−0.56	−1.26	−2.77	−2.61	4.31E−06
ASG-SP-64	Orlândia	−7.03	−46.21	0.79	0.36	−0.48	−1.23	−2.72	−2.40	2.76E−06
ASG-SP-65	Ipuã	−6.48	−43.49	0.70	0.27	−0.56	−1.96	−4.28	−2.61	3.05E−06
ASG-SP-66	Guará	−6.13	−41.34	0.49	0.07	−0.76	−1.68	−3.57	−2.53	8.14E−06
ASG-SP-67	Ituverava	nm	nm	0.59	0.17	−0.66	−0.71	−1.50	−2.87	3.22E−05
ASG-SP-68	Jeriquara	−6.93	−44.13	0.84	0.40	−0.44	−0.92	−2.16	−2.71	4.70E−06
ASG-SP-69	Igarapava	−6.52	−40.76	0.49	0.06	−0.77	−2.99	−5.98	−2.89	nd
ASG-SP-70	Miguelópolis	−8.87	−60.49	0.42	0.00	−0.83	0.16	0.14	−4.40	nd
ASG-SP-71	Guaíra	−5.73	−37.79	0.42	−0.01	−0.85	−0.04	−1.37	−4.71	nd
ASG-SP-72	Colômbia	−6.56	−41.44	0.98	0.55	−0.28	−0.82	−1.79	−2.41	3.00E−06
ASG-SP-73	Colômbia	nm	nm	0.89	0.46	−0.38	−0.50	−1.20	−2.96	9.31E−06
ASG-SP-74	Barretos	−6.82	−46.62	0.78	0.35	−0.48	0.19	0.02	−3.65	1.10E−04
ASG-SP-75	Jaborandi	−6.65	−43.20	0.89	0.46	−0.38	−0.82	−1.70	−2.92	7.33E−06
ASG-SP-76	Terra Roxa	−6.77	−43.82	0.85	0.42	−0.42	0.11	−0.18	−3.06	2.06E−05
ASG-SP-79	Viradouro	−6.41	−42.30	0.47	0.05	−0.78	−2.32	−4.70	−2.66	nd
ASG-SP-80	Morro Agudo	−8.58	−56.07	0.31	−0.10	−0.92	0.05	−0.46	−3.12	1.28E−04
ASG-SP-81	Cravinhos	−6.99	−43.11	0.86	0.42	−0.42	−0.79	−1.72	−2.80	nd
ASG-SP-82	Cravinhos	nm	nm	0.77	0.34	−0.51	−1.42	−2.88	−2.66	3.35E−06
ASG-SP-83	Barrinha	−8.79	−61.31	0.42	0.01	−0.82	−0.15	−0.98	−2.97	nd
ASG-SP-84	Pontal	−6.50	−44.46	0.49	0.08	−0.75	0.15	−1.05	−2.83	4.52E−05
ASG-SP-106	Araraquara	−7.28	−44.84	0.85	0.42	−0.42	−0.23	−0.71	−2.99	1.30E−05
ASG-SP-107	Am. Brasiliense	nm	nm	0.90	0.47	−0.37	−0.77	−1.55	−2.63	nd
ASG-SP-108	Am. Brasiliense	−6.98	−42.93	0.82	0.39	−0.44	−1.60	−3.00	−2.26	1.84E−06
Guaíra – GAS[a]	Guaíra	nm	nm	0.24	−0.17	−0.97	0.34	0.37	−4.20	nd
Rain	Rio Claro	nm	nm	−1.70	−2.12	−2.96	−5.46	−12.42	−2.62	nd

nm – not measured, nd – not determined.
[a] Extracted from Reis (2011).
[b] Al concentration calculated using PhreeqC.

dissolution of alumino-silicates in basalts can result in precipitation of carbonate minerals, kaolinite and SiO₂ polymorphs. There is possible mixing of groundwater from the underlying unit (Guarani Aquifer System), and to consider the effects of mixing, groundwater sampled in a GAS borehole by Reis (2011) in Guaíra (SP) was used to represent the composition of this end member in mixing simulations.

4. Results and discussion

4.1. Groundwater chemical composition

The amount of total dissolved solids of SGA groundwater varies from 0.76 to 6.75 mmol L^{-1}, and electric conductivity (EC) varies from 27.2 µS cm^{-1} to 370 µS cm^{-1} (arithmetic mean of 145 µS cm^{-1}), reflecting low content of solutes. Values of pH vary from 5.7 to 9.9 (arithmetic mean of 7.8), indicating the existence of acid and alkaline water in the aquifer. Table 3 summarizes the correlation between measured physico-chemical parameters. EC and pH have a strong correlation ($r = 0.80$) (Fig. 3), mainly related to the control exerted over pH by CO₂ and HCO₃ ($r = 0.76$ and 0.73, respectively), which represents the most abundant anion in SGA groundwater (Fig. 4), and explains the correlation between total alkalinity, EC and TDS ($r = 0.90$ and 0.92, respectively).

Dissolved oxygen (DO) varies from 7.12 to 0.51 mg L^{-1} (arithmetic mean of 4.55 mg L^{-1}), and samples showing values of DO lower than 2.00 mg L^{-1} (ASG-SP-15, ASG-SP-70 and ASG-SP-74) are located downgradient along flow paths, but it should be considered for the most part, groundwater are under oxidizing conditions. Samples with higher TDS have the lowest concentrations of dissolved oxygen (e.g. sample ASG-SP-15), Chloride and NO₃ concentrations show a wide range of values (from 0.001 to 0.293 µmol L^{-1} Cl and from <0.001 to 0.463 µmol L^{-1} NO₃), have a good correlation ($r = 0.65$), which could indicate an anthropogenic origin for these compounds due to leakage of sanitation systems as observed in some cities of São Paulo state (Bertolo et al., 2006). This origin is corroborated by the low correlation observed between Cl and Na ($r = 0.18$), excluding the possibility of groundwater recharge by precipitation affected by salt dissolution or evaporative enrichment of rainwater. Concentrations of Cl + NO₃ are greater than the concentration of SO₄ (usually <0.02 µmol L^{-1}), and only one sample (ASG-SP-15) has SO₄ with higher concentration. Dissolved cations are dominated by calcium and magnesium, which do not have a good correlation with TDS or total alkalinity. Sodium concentration increase is observed, strongly correlated with EC, TDS, pH and CO₃. The samples can be divided into two groups (Fig. 4). The first group is Ca–Mg–HCO₃ waters that have calcium as the most abundant cation, followed by magnesium, in variable relative concentrations, and with Ca/Mg ratios approaching 1. The second group is characterized by Na–HCO₃ waters that have higher TDS, compared to the average of Ca–Mg–HCO₃ waters (Fig. 4). It should be noted that some Ca–Mg–HCO₃ waters have TDS similar to those observed in Na–HCO₃ waters, indicating that they may be affected by processes related to dissolution of Ca and Mg minerals in basalts, and associated with cation exchange, one of the geochemical process associated with the origin of Na–HCO₃ waters (Drever, 1997; Appelo and Postma, 2005; Sracek and Hirata, 2002; Gastmans et al., 2010, among others).
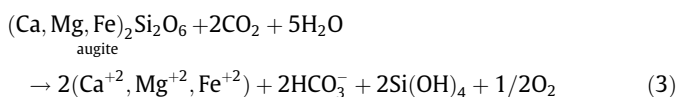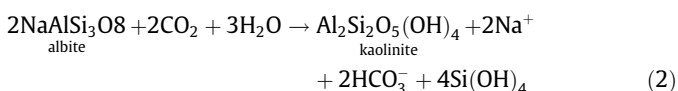
Table 3
Correlation matrix.

	EC	pH	HCO$_3$	CO$_3$	Alkalinity	Cl	NO$_3$	SO$_4$	F	Na	K	Ca	Mg	Si	TDS
EC	1.00	–	–	–	–	–	–	–	–	–	–	–	–	–	–
pH	**0.80**	1.00	–	–	–	–	–	–	–	–	–	–	–	–	–
HCO$_3$	**0.73**	0.61	1.00	–	–	–	–	–	–	–	–	–	–	–	–
CO$_3$	**0.76**	**0.79**	0.23	1.00	–	–	–	–	–	–	–	–	–	–	–
Alkalinity	**0.90**	**0.80**	**0.94**	0.55	1.00	–	–	–	–	–	–	–	–	–	–
Cl	0.40	0.03	0.02	0.17	0.08	1.00	–	–	–	–	–	–	–	–	–
NO$_3$	0.12	−0.39	0.05	−0.21	−0.03	**0.65**	1.00	–	–	–	–	–	–	–	–
SO$_4$	0.46	0.47	−0.01	0.50	0.17	0.61	−0.15	1.00	–	–	–	–	–	–	–
F	**0.67**	**0.68**	0.19	**0.73**	0.42	0.40	−0.19	**0.80**	1.00	–	–	–	–	–	–
Na	**0.81**	**0.88**	0.42	**0.92**	0.69	0.18	−0.22	0.51	**0.72**	1.00	–	–	–	–	–
K	−0.29	−0.34	−0.17	−0.32	−0.26	−0.12	0.02	−0.20	−0.27	−0.42	1.00	–	–	–	–
Ca	0.13	−0.20	0.49	−0.43	0.27	0.18	0.44	−0.23	−0.27	−0.44	0.12	1.00	–	–	–
Mg	−0.07	−0.40	0.13	−0.44	−0.04	0.24	0.56	−0.26	−0.27	−0.51	0.20	0.60	1.00	–	–
Si	0.32	0.17	0.26	0.06	0.25	0.41	0.22	0.29	0.28	0.05	−0.05	0.25	0.58	1.00	–
TDS	**0.98**	**0.85**	**0.76**	**0.74**	**0.92**	0.35	0.06	0.44	**0.64**	**0.84**	−0.33	0.07	−0.08	0.38	1.00

Correlation values in bold showing significance level $\rho < 0.001$.
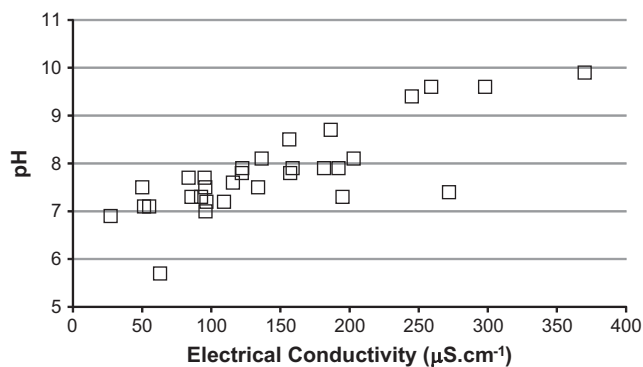
Fig. 3. Relationship between pH and electrical conductivity from SGA groundwater.

The geochemical evolution of groundwater may reflect water–rock interactions, and different relationships between the main cations and anions may then reflect specific water–rock reactions. If the trends observed represent reaction of groundwater with the basalt, with longer residence time higher TDS should be observed. Therefore, comparing cation and anion concentrations and the TDS may reflect the extent of water–rock reactions during the geochemical evolution of SGA groundwater. The dissolution of plagioclase and pyroxene, in the presence of atmospheric CO$_2$, can lead to secondary formation of kaolinite, releasing Ca, Na, Mg, Si and HCO$_3$ to solution. The incongruent dissolution of albite and anorthite, end members of the plagioclase feldspar series, (labradorite is intermediate in composition), and the dissolution of the pyroxene, augite, are presented below:

$$CaAl_2Si_2O_8 + 2CO_2 + 3H_2O \rightarrow \underset{kaolinite}{Al_2Si_2O_5(OH)_4} + Ca^{2+} + 2HCO_3^- \quad (1)$$
$$\underset{anorthite}{}$$

$$\underset{albite}{2NaAlSi_3O8} + 2CO_2 + 3H_2O \rightarrow \underset{kaolinite}{Al_2Si_2O_5(OH)_4} + 2Na^+$$
$$+ 2HCO_3^- + 4Si(OH)_4 \quad (2)$$

$$\underset{augite}{(Ca, Mg, Fe)_2Si_2O_6} + 2CO_2 + 5H_2O$$
$$\rightarrow 2(Ca^{+2}, Mg^{+2}, Fe^{+2}) + 2HCO_3^- + 2Si(OH)_4 + 1/2O_2 \quad (3)$$

As the mineral dissolution reactions consume CO$_2$ and produce HCO$_3$, a proportional increase in alkalinity with respect to TDS is expected, as observed in Fig. 5a. It should be noted that most samples are aligned with the correlation line (dashed), but some samples plot below the correlation line. The correlation observed for

most of the samples is due to the control exerted by pH over the alkalinity, and the samples that plot below the regression line present high nitrate and chloride concentration (samples ASG-SP-12 and ASG-SP-72, see Table 1), associated with anthropogenic contamination. Sample ASG-SP-15 has high concentrations of sulfate and chloride, under anoxic conditions (Table 1), which could be associated with pyrite dissolution and oxygen consumption.

The sum of cations (Na + Ca + Mg) is correlated with alkalinity (Fig. 5b), especially at concentrations below 1.5–2.0 mmol L^{-1}, with a ratio of 1:1, similar to the stoichiometric relationship observed in the sum of Eqs. (1)–(3). This is most likely related to dissolution of feldspars and pyroxene in basalts. The contribution of the dissolution of feldspars, releasing Ca and Na to groundwater, seems to be more important than the dissolution of pyroxenes, reflected by Mg. Concentrations of Mg show an increase similar to Na concentrations up to an alkalinity on the order of 1.5–2.0 mmol L^{-1}. With increasing alkalinity, the cations are mainly dominated by Na.

Besides the release of cations and HCO$_3$, basalt mineral weathering transfers silica into the water. The observed silica concentration in groundwater depends on mineralogical composition of the rocks, rate of dissolution, and immobilization of silica due to formation of secondary minerals, etc. (Appelo and Postma, 2005). Silica concentrations of SGA groundwater range from 0.25 to 1.05 mmol L^{-1}. All samples are oversaturated with respect to quartz (solubility of 0.18 mmol L^{-1} Si(OH)$_4$ at 25 °C; Rimstidt, 1997), saturated with respect to chalcedony (solubility of 1.35 mmol L^{-1} Si(OH)$_4$ at 25 °C; Fournier, 1977), but are undersaturated with respect to amorphous silica (solubility of 1.9 mmol L^{-1} Si(OH)$_4$ at 25 °C; Rimstidt and Barnes, 1980) (Table 3). If the source of silica is directly associated with basaltic mineral dissolution due to uptake of atmospheric CO$_2$, a stoichiometric relationship between concentrations of SiO$_2$ and HCO$_3$ should be expected (HCO$_3$:SiO$_2$ = 1:1 according to the stoichiometric sum of Eqs. (1)–(3), and represented as a dashed line in Fig. 5c). Some of the samples are aligned along a trend associated with continuous silicate dissolution, however many samples fall below the 1:1 ratio. Two geochemical processes may explain the observed relationship. As groundwaters become saturated with respect to quartz or chalcedony; removal of SiO$_2$ from the solution by secondary silica precipitation associated with precipitation of silica polymorphs or aluminous silicates (e.g., clay minerals) could be responsible for the decrease in silica concentration compared to alkalinity. The second process could be associated with preferential dissolution of anorthite, causing alkalinity to increase faster than silica content.
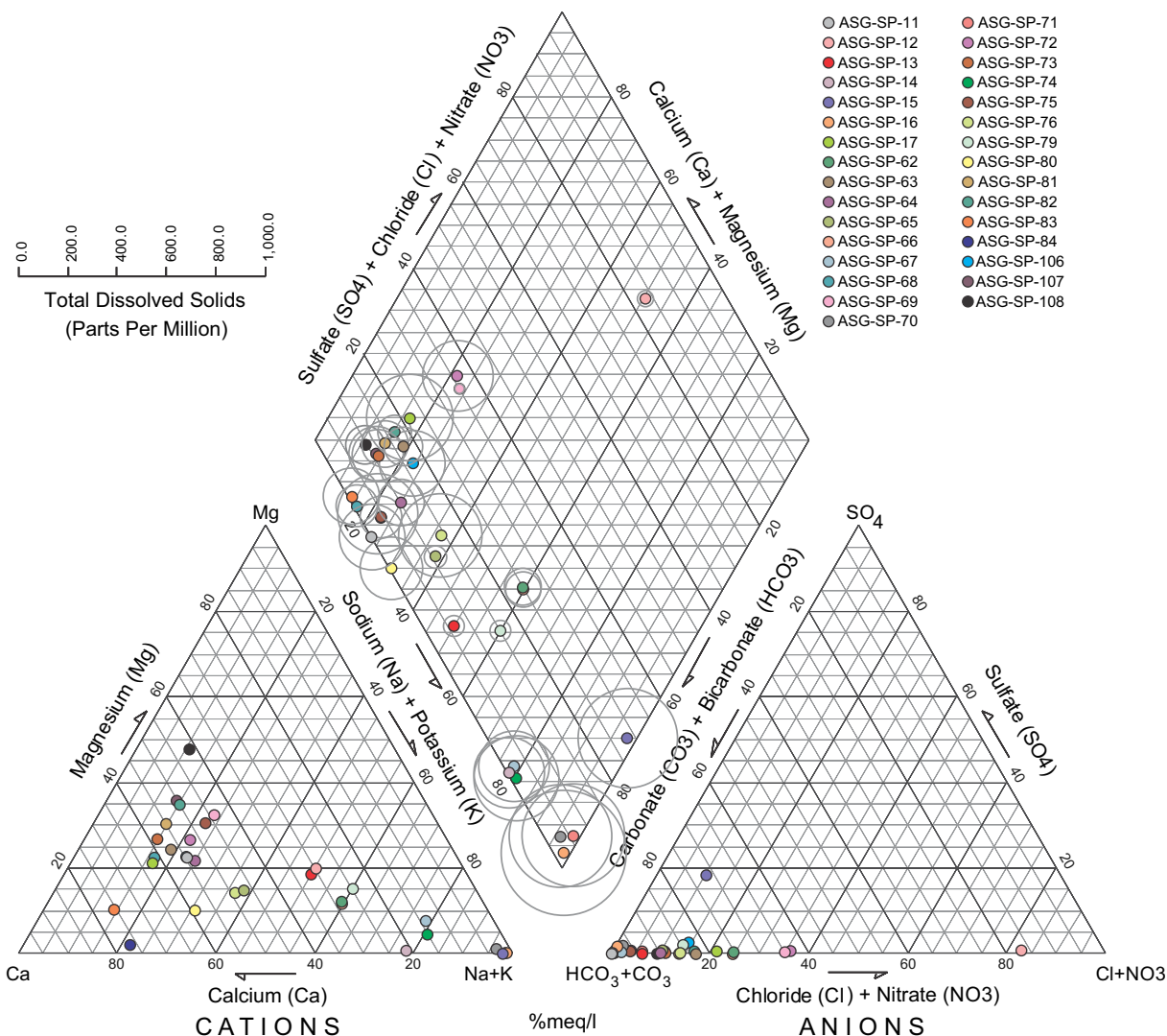
Fig. 4. Piper diagram.

Samples saturated or oversaturated with respect to calcite show a ratio of SiO_2:HCO_3 lower than the undersaturated samples, evidenced by their position in Fig. 5c (filled symbols). Despite saturation with calcite, alkalinity increases more than silica concentrations, which could be associated with another source of bicarbonate related to the existence of calcite, present filling vesicles in the basalts.

The continuous weathering of basalt, primarily by dissolution of plagioclase of labradorite composition, results in an increase in SiO_2, HCO_3, Na and Ca concentrations. As result of this continued dissolution of plagioclase, groundwater reaches calcite saturation. As Ca and HCO_3 are released with calcite dissolution, calcite equilibrium requires that HCO_3 increase and Ca decrease if calcite precipitates. Calcium concentrations increase at higher rates than Na concentrations up to Ca concentrations of about 1.0 mmol L^{-1} (Fig. 5d), where calcite saturation is reached. Ca concentrations then decrease as calcite precipitates, and Na concentration increases. This trend is interpreted to be associated mainly with feldspar (labradorite) dissolution, which, due to the release of Ca and HCO_3, could lead to saturation with respect to calcite. When calcite saturation is reached, feldspar dissolution still produces Ca, Na and HCO_3, but calcite precipitates, reducing the concentration of Ca (Fig. 5d) and the alkalinity increases relative to the sum of Na, Ca, and Mg (Fig. 5b).

Mineral dissolution associated with continuous uptake of atmospheric CO_2 occurs under open conditions, evidenced by calculated values of log pCO_2 about −2.5 to −3.0, controlling the constant increase in alkalinity (Fig. 6a). At this point, a decrease in pCO_2 is observed associated with calcite precipitation (Fig. 6b).

Equilibrium exchange reactions between Ca and Na can be represented using activity–activity diagrams, considering the production of smectite during basalt weathering (Clemente and Azevedo, 2007), and should be considered as possible exchange media. In order to understand the exchange process, Na-Beidellite and Ca-Beidellite are considered to be present in solid solution in smectite. Although the chemical composition of smectite in SGA basalt is not known, like most smectite minerals, it is probable that Na, Ca, Mg, K and H components are present. The groundwater samples generally follow the trend of the exchange boundary between Na- and Ca-Beidellite (smectite), but seem to deviate from this boundary near the laumontite phase boundary (Fig. 7). The samples that follow this steeper trend are typically saturated with respect to calcite. The trends observed suggest that ion exchange on smectite is possibly an important process controlling Na:Ca ratios in the SGA and that dissolution of laumontite (considered to be a higher temperature mineral) may affect compositions for more evolved samples.
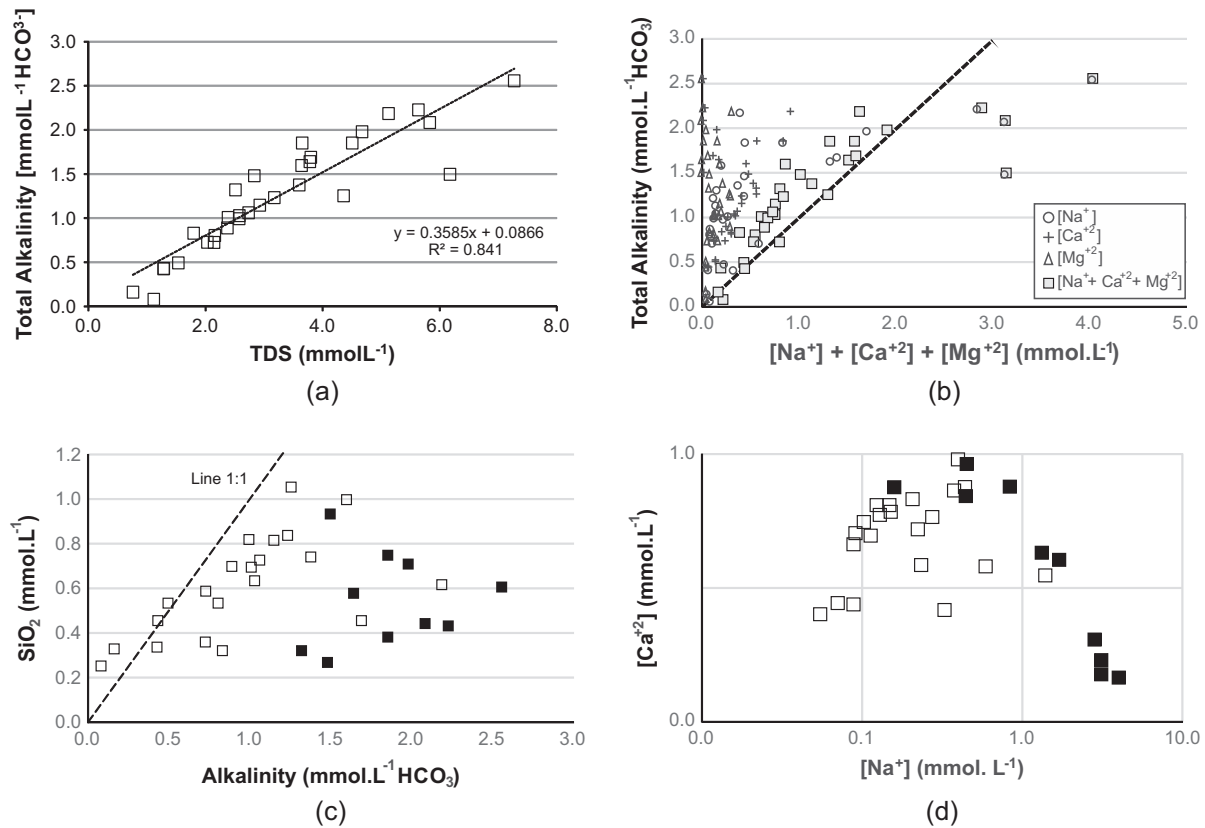
Fig. 5. (a) Relationship between TDS and total alkalinity (expressed as bicarbonate concentration) from SGA groundwater. Dashed line in the graph represents the best-fit correlation between TDS and total alkalinity. (b) Relationship between cations (Sodium, Calcium and Magnesium) concentrations and the alkalinity (expressed as bicarbonate concentration) from SGA groundwater. The dashed line represents the ratio 1:1, representing the sum of stoichiometric relations observed in Eqs. (1)–(3). (c) Relationship between silica and alkalinity (expressed as bicarbonate) Filled symbols represent samples saturated with respect to calcite (Table 2), and the dashed line (1:1) represents the sum of stoichiometric relations observed in Eqs. (1)–(3). (d) Relationship between sodium and calcium concentrations. Filled points indicate samples saturated or oversaturated with respect to calcite (data presented in Table 2).
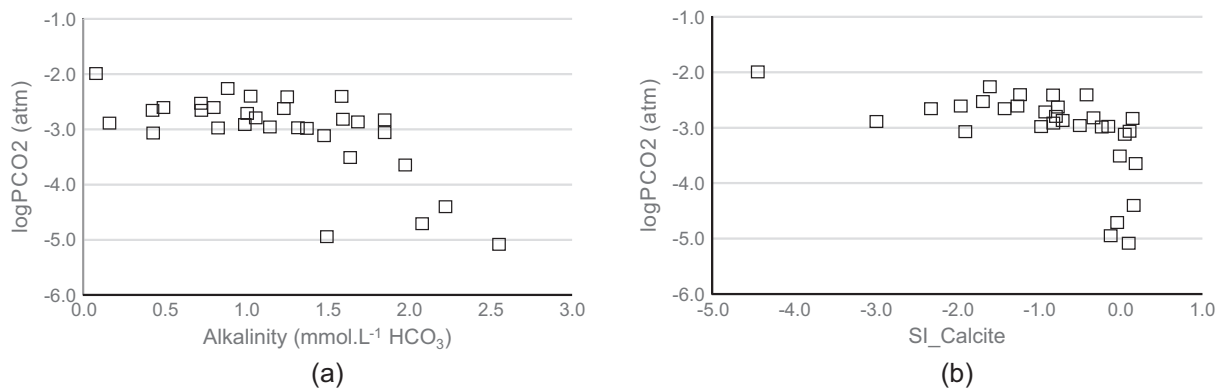

Fig. 6. Relationship between PCO_2 and alkalinity of SGA groundwater showing the continuous uptake of atmospheric CO_2 controlling the increase in alkalinity (a), when calcite saturation is reached, the consumption of CO_3 due to calcite precipitation decreases the PCO_2 (b).

4.2. Stable isotopes

The isotopic ratios of oxygen and hydrogen of samples from SGA groundwater are presented in Fig. 7, along with the Global Meteoric Water Line (GMWL) and the Brazilian Tropical Meteoric Water Line (BTMWL), given by the equation $\delta^2H = 7.7 \; \delta^{18}O + 10.1$ ($R^2 = 0.95$), derived from the GNIP data base. Cuiabá, Brasilia, Campo Grande, Rio de Janeiro, and Porto Alegre stations, located in the tropical region of Brazil, were selected due to weather conditions that are similar to those observed in the study area. Data

were collected between the 1960s and 1990s, and are available from the IAEA/WMO website (International Atomic Energy Agency/World Meteorological Organization), in the GNIP database (IAEA/WMO, 2006, accessed April 22th 2013). SGA groundwater has isotopic ratios ranging from −37.8‰ to −61.3‰ VSMOW for δ^2H, and −5.7‰ to −8.9‰ VSMOW for $\delta^{18}O$. Comparing groundwater to rainwater from GNIP stations shows that most groundwater has an isotopic signature similar to rainwater and plots near to the two meteoric lines, indicating a meteoric origin for the recharge of groundwater (Fig. 8).
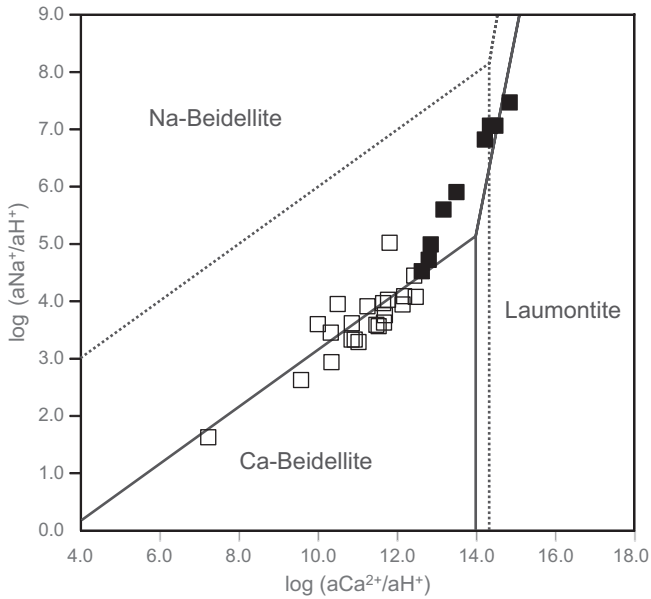
Fig. 7. Phase diagram in the system Na–Ca–Al–Si–O–H at 25 °C and 1.0 bar. Phases observed in the Serral Geral are allowed to be present. To account for the presence of other cations, two compositions were chosen and ideal mixing of components in smectite was assumed. Smectite with 0.2 mole fraction of K + Mg + H-Beidellite, 0.4 mole fraction of Na-Beidellite and 0.4 mole fraction of Ca-Beidellite is represented by the dashed phase boundaries. Solid lines indicate activity of Ca-Beidellite = 0.5, activity of Na Beidellite = 0.3. Dashed lines represent activity of Ca-Beidellite = activity of Na Beidellite = 0.4. Filled points indicate samples saturated with respect to calcite (data presented in Table 2).

Distinct isotopic ratios suggest two groups of groundwater in SGA. The first group is represented by more depleted water, with values of δ^{18}O up to $-8.5‰$ VSMOW. The second group encompasses the most enriched samples, with δ^{18}O varying from $-5.8‰$ to $-7.5‰$ VSMOW, similar to present day precipitation. These observed variations indicate that groundwater recharge may have occurred under different climatic conditions, related to the intensity of the monsoonal system acting over the South American continent. Most of the SGA groundwater samples have compositions related to present day precipitation observed at Campo Grande GNIP station, but more depleted than the weighted mean values observed at Cuiaba, Brasilia, Rio de Janeiro and Porto Alegre GNIP stations (Fig. 8). Depleted values (δ^{18}O ≈ $-8.0‰$ VSMOW) are similar to those recognized in Guarani Aquifer groundwater collected from wells located in the study area by several authors

(e.g. Gallo and Sinelli, 1980; Kimmelmann e Silva et al., 1982; Gastmans et al., 2013; Chang et al., 2013, among others).

Variations of precipitation isotopic ratios are associated with climatic controls in the tropical region of Brazil. These are primarily driven by the interaction of tropical and extra-tropical air masses, which are responsible for the patterns of precipitation over this zone, such as changing sources representing summer and winter rainfalls. This interannual variability is related to the migration of the Intertropical Convergence Zone (ITCZ) (Rosanski and Araguás-Araguás, 1995). Due to the position of ITCZ during the summer (November–March), precipitation over the continent is controlled by a monsoonal regime (South America Summer Monsoon – SAMS) that is responsible for over 50% of the annual amount of rainfall over the continent, presenting as major vapor sources water evaporated over the Amazon region, producing more depleted precipitation. Winter and late spring precipitation (May–September) are related to an extratropical circulation system producing isotopically more enriched precipitation (Vuille and Werner, 2005; Vuille et al., 2003). Variations of the ITCZ movement, which would extend further south of the South American continent, produce more intense and depleted precipitation, as observed by Cruz et al. (2005) who examined the isotopic composition of drip water and speleothems in caves located in the southern part of the state of São Paulo. The observed isotopic ratios for the bulk of SGA groundwater are more depleted than recent precipitation over the Tropical Region of Brazil (values for δ^{18}O varies from $-6.0‰$ to $-7.0‰$ VSMOW), indicating an important recharge contribution related to precipitation associated with the SASM, a major vapor source associated with recirculation over the Amazon region.

4.3. Geochemical evolution for SGA groundwater and mass balance approach

NETPATH XL mass balance modeling was used with water chemistry and knowledge of the primary and secondary minerals present in the Serra Geral and the overlying soil to examine the mineral reactions responsible for the evolution of Serra Geral groundwater. In the following discussion, flow paths are discussed with reference to both the results from NETPATH XL, and the water chemistry. The isotope data show that low TDS rainwater has infiltrated the Serra Geral and reacts with the basalt minerals and soils, producing high TDS waters as water–rock reactions proceed. The resulting trend from low TDS water to high TDS water is not spatially uniform because in some places, local groundwater
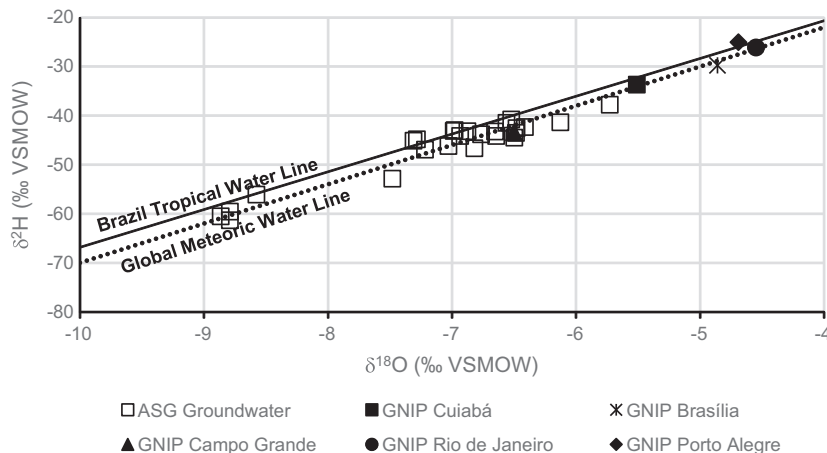
Fig. 8. δ^{18}O versus δ^{2}H cross plot for SAGS groundwater from the study area. Brazilian Tropical Meteoric Water Line (BTMWL solid line) and Global Meteoric Water Line (GMWL dashed line) are shown, as well as the long term weighted isotopic ratios for the selected GNIP stations.
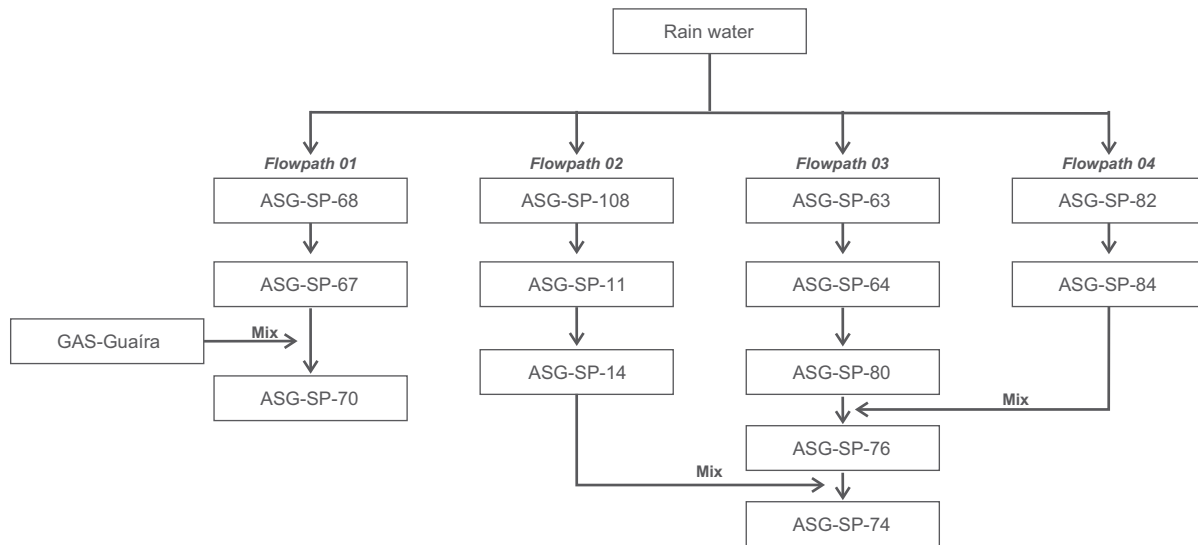
Fig. 9. Selected wells to perform mass balance simulation along the flow paths.

circulation determined by the discontinuities in basaltic rocks has allowed infiltration of low TDS water near to areas where high TDS water is present. Therefore, wells selected for NETPATH XL simulation show continuously increasing TDS along the flow paths. Schematic distribution of selected wells along the flow paths is presented in Fig. 9.

Constraints considered in the mass balance simulation were: calcium, sodium, magnesium, silicon, carbon and aluminum. These constrains determine the maximum number and types of phases involved in the simulation. As aluminum concentrations in most part of samples are below the limit of detection of the analytical method (<0.0002 mmol L^{-1}), concentrations were calculated using PhreeqC by considering these groundwaters to be in equilibrium with kaolinite. The results are presented in Table 2. The complete phase-list is presented in Table 4.

The starting end member for all NETPATH XL simulations is rainwater, represented by the average chemical composition of eleven rain events sampled in Rio Claro (SP) during 2013. Chemical changes in SGA groundwater related to rainwater recharge along the evaluated flowpaths reflect the dissolution of feldspars, represented mainly by labradorite (An 70 Ab 30), pyroxenes (augite), and uptake of atmospheric CO_2. Dissolution of Mg-montmorillonite present in the soil and produced by weathering of basalts can contribute minor amounts of Mg to groundwater, as observed in flow paths 02 and 04, but the dissolution of augite releases more Mg than the observed concentrations. Clay minerals appear to be the sink for this element, here simulated as chlorite. Kaolinite precipitates, as suggested by reactions (1) and (2), due to incongruent dissolution of feldspars, as well as quartz, consistent with SI calculations from the water chemistry data.

The evolution of groundwater in the basaltic aquifer under open conditions (log pCO$_2$ about −2.5 atm), leads to the continuous incongruent dissolution of labradorite and augite, leading to kaolinite and quartz precipitate, as previously discussed. These reactions were modeling between the wells ASG-SP-68 to ASG-SP-67 (FP 01), ASG-SP-108 to ASG-SP-11 (FP 02), ASG-SP-63 to ASG-SP-64 and ASG-SP-64 to ASG-SP-80 (FP 03) and ASG-SP-82 to ASG-SP-84 (FP 04). Otherwise, along the flow paths there is a substantial increase of Na and decrease in Ca, which in the simulation is related to equilibrium-exchange reactions associated with clay minerals, as previously suggested. With NETPATH XL, this reaction was modeled as forward exchange, and the results are shown in Table 4. The continuous uptake of CO_2, considered to

dissolve in NETPATH XL modeling, does not allow saturation with respect to calcite for the resulting water in the flow paths evaluated.

Groundwater evolves under closed conditions from well ASG-SP-11 to ASG-SP-14 (FP 02), where the basalts are overlaid by sediments of Bauru Group, and NETPATH XL suggests that the chemical evolution of this segment of the flow path is best explained by labradorite and augite dissolution associated with exchange processes, resulting in and the increase in Na concentration, accompanied by quartz (or a silica polymorph), calcite and chlorite precipitation.

Chemical evolution involving the mixture of flow paths 03 and 04, respectively represented by the wells ASG-SP-80 and ASG-SP-84, reaching well ASG-SP-76, were modeled with NETPATH XL considering an uptake of atmospheric CO_2, consistent with log pCO$_2$ calculated for the samples involved in this mixture (about −3.0). The atmospheric CO_2 dissolves augite and exchange processes are responsible for the variations in cation concentrations (increase in Na and a decrease in Ca and Mg). Quartz or a silica polymorph precipitates due to saturation of groundwater with respect to this mineral, and precipitation is responsible by keeping silica concentrations almost constant. The excess of Mg produced is controlled by the precipitation of clay minerals, modeled as chlorite. The mixing calculation indicates a primary contribution from flow path 03 (0.61:0.39).

Composition of the end member groundwater ASG-SP-74 represents the mixture of two flow paths (02 and the mixture of 03 and 04). Part of this pathway is under open conditions (ASG-SP-76 to ASG-SP-74), where the basalts outcrop, while the other pathway is under closed conditions (ASG-SP-14 to ASG-SP-74). The geochemical processes during mixing were modeled to involve the uptake of CO_2 (0.051 mmol kg^{-1}), labradorite dissolution, and cation exchange, to represent the increase in Na, and decrease in Ca. The percentage of mixture is about 0.11:0.89 (ASG-SP-14: ASG-SP-76).

The final step of groundwater evolution along flow path 01, represented by sample ASG-SP-70, was modeled to evolve under CO_2 closed conditions, in accordance to calculated log pCO$_2$ about −4.1 for water samples. The observed higher pressure head measured in wells drilled in the Guarani Aquifer System, in the downstream area of the main rivers in the studied area (Sapucaí, Pardo and Grande), indicates that this unit is under confining conditions, allowing for the possibility of groundwater flow into the overlying

Table 4
Mass transfer, calculated with NETPATH (Plummer et al., 1994) for net hydrochemical reactions along selected flow paths (in mmol kg^{-1}).

	Flow Path 01		Flow Path 02				Flow Path 03			Flow Path 04		Mix 03/04	Mix 03/04-02
Water #1	Rain	ASG-SP-68	ASG-SP-67	Rain	ASG-SP-108	ASG-SP-11	Rain	ASG-SP-63	ASG-SP-64	Rain	ASG-SP-82	ASG-SP-84	ASG-SP-14
Water #2	ASG-SP-68	ASG-SP-67	GAS-Guaíra	ASG-SP-108	ASG-SP-11	ASG-SP-14	ASG-SP-63	ASG-SP-64	ASG-SP-80	ASG-SP-82	ASG-SP-84	ASG-SP-80	ASG-SP-76
End Member	ASG-SP-68	ASG-SP-67	**ASG-SP-70**	ASG-SP-108	ASG-SP-11	ASG-SP-14	ASG-SP-63	ASG-SP-64	ASG-SP-80	ASG-SP-82	ASG-SP-84	ASG-SP-76	**ASG-SP-74**
Dissolution (mmol kg^{-1})													
CO_2 gas	0.967	0.644		0.972	0.555		0.782	0.280	0.309	0.698	1.072	0.214	0.051
Labradorite	0.247	0.065	0.271	0.171	0.231	0.077	0.194	0.116	0.044	0.215	0.673		0.051
Augite	0.525	0.888	0.044	0.384	0.222	0.667	0.492	0.064	0.503	0.302	0.651	0.352	
Mg-Montmorilonite				0.035				0.056	0.074	0.066			
Exchange		0.615				0.539						0.195	0.390
Precipitation (mmol kg^{-1})													
Kaolinite	0.241		0.267	0.247	0.197		0.191	0.114		0.306	0.604		0.031
SiO_2	0.140	1.595	0.178		0.021	1.411	0.250		1.130		1.181	0.126	
Calcite			0.008	0.003		0.045							
Chlorite	0.058	0.154			0.057	0.143	0.052	0.009	0.091	0.016		0.035	0.020
Mixing proportions													
Initial water #1			0.121									0.390	0.110
Initial water #2			0.879									0.610	0.890

basalts (Fig. 2). The thickness of basalts in Miguelópolis is about 200 m, increasing westward, reaching up to 600 m in Barretos. This upward groundwater flow from GAS to SGA has been assumed to occur in several portions of the Paraná Sedimentary Basin, especially where the basalt layer is thicker, as pointed out by da Silva (1983), Rebouças (1994), Buchmann Filho et al. (2002), Gastmans and Chang (2012), among others. In addition to the data for hydraulic head, there are similarities between the chemical composition and isotopic content of the sample ASG-SP-70 to groundwater sampled in Guaíra (GAS-Guaíra). Both are Na–HCO_3 groundwater types with low values of pCO_2 (log pCO_2 about −4.0) and are saturated with respect to calcite. They also are associated with depleted values of $\delta^{18}O$ (about −8.5‰ VSMOW). This suggests that one of the processes influencing the chemical and isotopic composition of the SGA groundwater, especially downgradient towards Rio Grande, is the continuous intrusion and mixing of groundwater derived from the Guarani Aquifer System (GAS). Simulations performed using NETPATH without a component of mixing results in models that do not fit the observations as well as models that have mixing included. The estimated proportion of mixing is about 0.12:0.88 (SGA:GAS). Sample ASG-SP-70 is saturated with respect to calcite and evolves towards a CO_2 closed system. Calculations suggest labradorite and a small amount of augite are dissolved, and calcite, kaolinite and chlorite are precipitated.

5. Conclusions

The evaluation of new hydrochemical and stable isotopic data for groundwaters of the Serra Geral Aquifer in the northern portion of São Paulo state (BR), using isotopic and geochemical methods, has contributed to the recognition of the main geochemical process and controls related to groundwater evolution within this basaltic reservoir. Groundwater flow in the Serra Geral aquifer is driven by the topography, and the main rivers crossing the area represent local areas of discharge. High pressure head in wells drilled in the Guarani Aquifer System indicate that this unit is under confining conditions, as well as suggesting the possibility of groundwater flow into the overlying basalts.

Groundwaters from SGA have low content in solutes, reflected by the low values of TDS, and neutral to alkaline pH's. HCO_3 is the major anion and calcium and magnesium the major cations, but an increase in sodium concentrations is observed associated with increasing TDS.

Stable isotope ratios measured in SGA groundwater vary from −37.8‰ to −61.3‰ VSMOW for δ^2H and −5.7‰ to −8.9‰ VSMOW for $\delta^{18}O$, with an isotopic signature similar to rainwater, indicating a meteoric origin for the recharge of these groundwaters. More depleted values are associated with climatic controls in the tropical region of Brazil, and are similar to those observed in the confined zone of the Guarani Aquifer System.

Groundwater composition is directly related to water–rock interactions, mainly due to the dissolution of plagioclase (labradorite) and pyroxene (augite) (rock forming minerals), in the presence of atmospheric CO_2, leading to secondary formation of kaolinite, quartz and clay minerals, and releasing calcium, sodium, magnesium, silica and bicarbonate to solution. Under open conditions groundwater does not reach calcite saturation and increases in sodium concentration are interpreted to result from equilibrium exchange reactions consistent with the exchange boundary between Na and Ca Beidellite (smectites). Under closed conditions the consumption of CO_2 lead to calcite precipitation, contributing to a relative increase in Na concentrations.

The possible reactions expected to occur during geochemical evolution have been tested using NETPATH XL (Plummer et al., 1994; Parkhurst and Charlton, 2008), constrained by the observed

mineralogy and chemical and isotopic data from the SGA. Where the aquifer is unconfined, direct recharge of meteoric waters in the basalts causes groundwater to evolve in a CO_2 open system, shown mainly by the evolution of the concentrations of calcium, magnesium and bicarbonate released into groundwater by mineral dissolution and leading to neutral pH. Model results suggest dissolution of basalt minerals along the flow paths evaluated, primarily feldspar (approximating labradorite composition) and augite. In addition, dissolution of clay minerals present in the soil, acts as a supplementary source for Mg in recharge zone. Controls over Ca, Na and Mg in the basaltic aquifer are related to equilibrium exchange reactions and the formation of Mg-clay mineral, simulated to be chlorite. SGA Groundwater flow down gradient leads to confining conditions, and geochemical evolution occurs in a system closed to CO_2, the occurrence of which is coincident with mixing of groundwater from the underlying Guarani Aquifer System.

Flow and the resulting mixing between the main aquifers of the Paraná Basin: Bauru, Serra Geral and Guarani, is an important control on the composition of basaltic groundwater. This study reveals the importance of regional groundwater flow in complex hydrogeological systems, similar to the Paraná Basin that are comprised of aquifers that may interact, superimposed on geochemical processes.

Acknowledgment

References

Aggarwal, P.K., Gat, J.R., Froehlich, K.F.O. (Eds.), 2005. Isotopes in the Water Cycle – Past Present and Future of a Developing Science. Springer, Netherlands, 377p.

Appelo, C.A.J., Postma, D., 2005. Geochemistry, Groundwater and Pollution, second ed. Balkema Publishers, Amsterdam, 650p.

Barison, M.R., 2003. Estudo Hidroquímico na Porção Meridional do Sistema Aquífero Bauru no Estado de São Paulo. Tese (Doutorado em Geociências e Meio Ambiente). Instituto de Geociências e Ciências Exatas, UNESP, Rio Claro (SP), 153p.

Bellieni, G., Comin-Chiaromonti, P., Marques, L.S., Melfi, A.J., Nardy, A.J., Papatrechas, C., Piccirilo, E.M., Roisemberg, A., 1986. Petrogenetic aspects of acid and basaltic lavas from the Paraná Plateau (Brazil): geological, mineralogical and petrochemical relationships. J. Petrol. 27, 915–944.

Bertolo, R., Hirata, R., Sracek, O., 2006. Geochemistry and geochemical modeling of unsaturated zone in tropical region in Urânia, São Paulo state, Brazil. J. Hydrol. 329, 49–62.

Bethke, C.M., 2007. The Geochemist's Workbench® Release 7.0 (four volumes). Hydrogeology Program, University of Illinois, Urbana, Illinois.

Bittencourt, A.V.L., 1996. Sobre o controle do quimismo de águas termais da Bacia do Paraná. Boletim Paranaense de Geociências 44, 117–129.

Bittencourt, A.V.L., Rosa Filho, E.F., Hindi, E.C., Buchmann Filho, A.C., 2003. A influência dos basaltos e de misturas com águas de aquíferos sotopostos nas águas subterrâneas do Sistema Aquífero Serra Geral na Bacia do Rio Piquiri, Paraná – BR. Revista Águas Subterrâneas 17, 67–75.

Boff, F.E., Medeiros, M.A., Muller, A.L., Koppe, J.C., 2006. Caracterização hidroquímica das águas minerais da Serra do Nordeste Gaúcho. In: Congresso Brasileiro de Águas Subterrâneas, 14, 2006. ABAS, Curitiba, 18p. (CD-ROOM).

Bouhlassa, S., Aiachi, A., 2002. Groundwater dating with radiocarbon: application to an aquifer under semi-arid conditions in the south of Morocco (Guelmine). Appl. Radiat. Isotopes 56, 637–647.

Bourlier, P.Y., Lachassagne, P., Desprats, J.F., Gille, E., 2005. Nouveaux Éléments sur la Structure et le Fonctionnement Hydrogéologique du Plateau Basaltique de L'Aubrac (Massif Centrel, France). Première Évaluation dês Potentialités em Eau Souterraine. C. R. Geosci. 337, 663–673.

Bretzler, A., Osenbrück, K., Gloaguen, R., Ruprecht, J., Kebede, S., Stadler, S., 2011. Groundwater origin and flow dynamics in active rift system – a multi-isotope approach in the Main Ethiopian Rift. J. Hydrol. 402, 274–289.

Buchmann Filho, A.C., Rosa Filho E.F., Hindi, E.C., Bittencourt, A.V.L., Nadal, C.A., Ferreira, F.J.F., 2002. Aspectos da Química da Água Subterrânea da Formação Serra Geral no Âmbito da Bacia Hidrográfica do Rio Piqueri (PR). In: Congresso Brasileiro de Águas Subterrâneas, 12, 2002. ABAS, Florianópolis, 17p. (CD-ROOM).

Campos, H.C.N.S., 1987. Contribuição ao Estudo Hidrogeoquímico do Grupo Bauru no Estado de São Paulo. Dissertação de Mestrado. Instituto de Geociências, Universidade de São Paulo, São Paulo (SP), 105p.

Campos, H.C.N.S., 1993. Caracterização e Cartografia das Províncias Hidrogeoquímicas do Estado de São Paulo. Tese de Doutoramento. Instituto de Geociências, Universidade de São Paulo, São Paulo (SP), 177p.

Chang, H.K., Aravena, R., Gastmans, D., Hirata, R., Manzano, M., Vives, L., Rodrigues, L., Aggarwal, P., Araguas, L., 2013. Role of isotopes in the development of a general hydrogeological conceptual model of the Guarani Aquifer (GAS). In: International Atomic Energy Agency (Org.). Isotopes in Hydrology, Marine Ecosystems and Climate Change Studies, vol. 2, first ed. International Atomic Energy Agency, Viena, pp. 281–290.

Clemente, C.A., Azevedo, A.C., 2007. Mineral weathering in acid saprolites from Subtropical, Southern Brazil. Sci. Agricola (Piracicaba, Brazil) 64 (6), 601–607.

Cruz, F.W., Karmann, I., Viana Jr., O., Burns, S.J., Ferrari, J.A., Vuille, M., Sial, A.N., Moreira, M.Z., 2005. Stable isotope study of cave percolationwaters in subtropical Brazil: implications for paleoclimate inferences from speleothems. Chem. Geol. 220, 245–262.

Departamento de Águas e Energia Elétrica do Estado de São Paulo, 1974. Estudo de Águas Subterrâneas. Região Administrativa 6 – Ribeirão Preto, vol. 2. DAEE, São Paulo (Texto).

Departamento de Águas e Energia Elétrica do Estado de São Paulo, 1976. Estudos de Água Subterrânea. Regiões Administrativas 7, 8, 9 (Bauru, São José do Rio Preto, Araçatuba), vol. 2. DAEE, São Paulo (Texto), 286p.

Departamento de Águas e Energia Elétrica do Estado de São Paulo/Universidade Estadual Paulista, 1980. Mapa Geológico do Estado de São Paulo scale 1:250,000. São Paulo.

Dafny, E., Gvirtzman, H., Burg, A., Fleischer, L., 2003. The hydrogeolgy of the Golan Basalt aquifer, Israel. Israel J. Earth Sci. 52, 139–153.

Dafny, E., Burg, A., Gvirtzman, H., 2006. Deduction of groundwater flow regime in a basaltic aquifer using geochemical and isotopic data: the golan heights, Israel case study. J. Hydrol. 330, 506–524.

Deolankar, S.B., 1980. The Deccan Basalts of Maharashtra, India – their potential as aquifers. Ground Water 18 (5), 434–437.

Deutsch, W.J., Jenne, E.A., Krupka, K.M., 1982. Solubility equilibria in basalt aquifers: the Columbia Plateau, Eastern Washington, USA. Chem. Geol. 36, 15–34.

Domenico, P.A., Schwartz, F.W., 1998. Physical and Chemical Hydrogeology. John Wiley & Sons, New York, 824p.

Drever, J.I., 1997. The Geochemistry of Natural Waters: Surface and Groundwater Environments. Prentice Hall, Upper Saddle River, p. 435.

Ernesto, M., Raposo, M.I.B., Marques, L.S., Renne, P.R., Diogo, L.A., de Min, A., 1999. Paleomagnetism, geochemistry and $^{40}Ar/^{39}Ar$ dating of the northeastern Paraná Magmatic Province: tectonic implications. J. Geodyn. 28, 321–340.

Fernandes, A.J., Maldaner, C.H., Sobrinho, J.M.A., Pressinotti, M.M.N., Wahnfried, I., 2010. Estratigrafia dos derrames de basaltos da Formação Serra Geral (Ribeirão Preto-SP) baseada na geologia física, petrografia e geoquímica. Revista do Instituto de Geociências – USP, vol. 10(2), pp. 73–99.

Fournier, R.O., 1977. Chemical geothermometers and mixing models for geothermal systems. Geothermics 5 (1–4), 41–50.

Frank, H.T., 2008. Gênese e padrões de distribuição de minerais secundários na Formação Serra Geral (Bacia do Paraná). Tese (Doutorado em Geociências). Instituto de Geociências, UFRGS, Porto Alegre (RS), 324p.

Gallo, G., Sinelli, O., 1980. Estudo Hidroquímico e Isotópico das Águas Subterrâneas na Região de Ribeirão Preto (SP). Revista Brasileira de Geociências 10, 129–140.

Gastmans, D., Chang, H.K., Hutcheon, I., 2010. Groundwater geochemical evolution in the northern portion of the Guarani Aquifer (Brazil) and its relationship to diagenetic features. Appl. Geochem. 25, 16–33.

Gastmans, D., Chang, H.K., Aggarwal, P., Sturchio, N., Araguas, L., 2013. Groundwater ages and hydrochemical evolution along a flow-path in the northeastern sector of the Guarani Aquifer (GAS) derived from structural geology, isotopes and hydrochemical data. In: International Atomic Energy Agency (Org.). Isotope in Hydrology, Marine Ecosystems and Climate Change Studies, vol. 2, first ed. International Atomic Energy Agency, Viena, pp. 271–279.

Gastmans, D., Chang, H.K., 2012. Circulação das Águas Subterrâneas do Sistema Aquífero Guarani nas Proximidades da Zona de Afloramento no Estado de São Paulo. In: Congresso Brasileiro de Águas Subterrâneas, 17, 2012. ABAS, Bonito, 4p. (CD-ROOM).

IAEA/WMO, 2006. Global Network of Isotopes in Precipitation: the GNIP database. IAEA/WMO, Vienna. <http://isohis.iaea.org> (Cited 22 April 2013).

Kimmelmann e Silva, A.A., Rebouças, A.C., Santiago, M.M.F., Silva, R.B.G., 1982. Isotopic study of the Botucatu Aquifer system in the Brazilian portion of the Parana Basin. In: Isotope Hydrology Investigations in Latin America (IAEE-TECDOC – 502), pp. 51–71.

Kimmelmann e Silva, A.A., Silva, R.B.G., Rebouças, A.C., Santiago, M.M.F., 1986. Hidrologia Isotópica do Aqüífero Botucatu – Bacia do Paraná – Brasil. In: Congresso Brasileiro de Hidrogeologia, 4, 1986. ABAS, Brasília, pp. 1–25.

Kulkarni, H., Deolankar, S.B., Lawwani, A., Joseph, B., Pawar, S., 2000. Hydrogeological framework of the Deccan basalt groundwater systems, West-central India. Hydrogeol. J. 8, 368–378.

Lastoria, G., 2002. Hidrogeologia da Formação Serra Geral no Estado de Mato Grosso do Sul. Tese (Doutorado em Geociências e Ciências Exatas). Instituto de Geociências e Ciências Exatras, Universidade Estadual Paulista, Rio Claro, 197p.

Lastoria, G., Sinelli, O., Chang, H.K., Hutcheon, I., Paranhos Filho, A.C., Gastmans, D., 2006. Hidrogeologia da Formação Serra Geral no Estado de Mato Grosso do Sul. Águas Subterrâneas 20, 139–150.

Léonardi, V., Arthaud, F., Grillot, J.C., Avetissian, V., Bochnaghian, P., 1996. Modélisation d'un Aquifère Basaltique Fracturé Tenant Comptes de Données Géologiques, Climatiques et Hydrauliques: Cas de Basaltes Perchés de Garni (Arménie). J. Hydrol. 179, 87–109.

Locsey, K.L., Cox, M.E., 2003. Statistical and hydrochemical methods to compare basalt and basement rock hosted groundwaters: Atherton Tablelands, Northeastern Australia. Environ. Geol. 43, 698–713.

Machado, J.L.F., Freitas, M.A., Caye, B.R., 2002. Evolução Hidrogeoquímica dos Aquíferos no Oeste Catarinense. In: Congresso Brasileiro de Águas Subterrâneas, 12, 2002. ABAS, Florianópolis, 10p. (CD-ROOM).

Machado, F.B., 2007. Petrologia e Caracterização Geoquímica das Fontes Mantélicas da Região Noroeste da Província Magmática do Paraná. Tese (Doutorado em Geologia Regional). Instituto de Geociências e Ciências Exatas, Universidade Estadual Paulista, Rio Claro, 260p.

Machado, F.B., Nardy, A.J.R., Oliveira, M.A.F., 2007. Geologia e Aspectos Petrológicos das Rochas Intrusivas e Efusivas Mesozóicas de Parte da Borda Leste da Bacia do Paraná no Estado de São Paulo. Revista Brasileira de Geociências 37 (1), 64–80.

Meng, S.X., Maynard, J.B., 2001. Use of statistical analysis to formulate conceptual models of geochemical behavoir: water chemical data from the Botucatu Aquifer in São Paulo State, Brazil. J. Hydrol. 250, 78–87.

Milani, E.J., França, A.B., Schneider, R.L., 1994. Bacia do Paraná. Boletim de Geociências da Petrobrás 8 (1), 69–82.

Nanni, A.S., 2008. O Flúor em Águas do Sistema Aquífero Serra Geral no Rio Grande do Sul: Origem e Condicionamento Geológico. Tese de Doutorado. Instituto de Geociências, Universidade Federal do Rio Grande do Sul, Porto Alegre, 127p.

Nardy, A.J.R., Oliveira, M.A.F., Betancourt, R.H.S., Verdugo, D.R.H., Machado, F.B., 2002. Geologia e Estratigrafia da Formação Serra Geral. Revista Geociências 21 (2), 15–32.

Paula e Silva, F.S., Chang, H.K., Caetano-Chang, M.R., 2005. Hidroestratigrafia do Grupo Bauru (K) no Estado de São Paulo. Águas Subterrâneas 19 (2), 19–36.

Parkhurst, D.L., Appelo, P., 1999. User's Guide to PHREEQC (Version 2) – A Computer Program for Speciation, Speciation, batch-reaction, one-dimensional transport and inverse geochemical calculations. USGS, 1999. U.S. Geological Survey Water-Resources Investigations Report 99-4259, 310p.

Parkhurst, D.L., Charlton, S.R., 2008. NetpathXL – An Excel® Interface to the Program NETPATH. U.S. Geological Survey Techniques and Methods 6-A26, 11p.

Plummer, L.N., Busby, J.F., Lee, R.W., Hanshaw, B.B., 1990. Geochemical modeling of the Madison Aquifer in parts of Montana, Wyoming and South Dakota. Water Resour. Res. 26 (9), 1981–2014.

Plummer, L.N., Prestemon, E.C., Parkhurst, D.L., 1994. An interactive code (NETPATH) for modeling NET geochemical reactions along a flow PATH, version 2.0. U.S. Geological Survey Water-Resources Investigations Report 94-4169, 130 p.

Rebouças, A.C., Sistema Aquífero Botucatu no Brasil. In: Congresso Brasileiro de Águas Subterrâneas, 8, Recife. Anais....Recife, pp. 500–509.

Rebouças, A.C., Fraga, C.G., 1988. Hidrogeologia das rochas vulcânicas do Brasil. Revista Brasileira de Águas Subterrâneas 12, 29–55.

Reis, M.M., 2011. Potencial Hidrotermal das Águas Hipertermais do Sistema Aquífero Guarani no Estado de São Paulo. Tese (Mestrado em Geociências e Meio Ambiente). Instituto de Geociências e Ciências Exatas, Universidade Estadual Paulista, Rio Claro, 116p.

Renne, P.R., Ernesto, M., Pacca, I.G., Coe, R.S., Glen, J.M., Prévot, M., Perrin, M., 1992. The age of Paraná flood volcanism, rifting of Gondwanaland, and the Jurassic-Cretaceous Boundary. Science 258, 975–979.

Renne, P.R., Deckart, K., Ernesto, M., Féraud, G., Piccirillo, E.M., 1996. Age of the Ponta Grossa dike swarm (Brazil), and implications to Paraná flood volcanism. Earth Planet. Sci. Lett. 144, 199–211.

Rimstidt, J.D., 1997. Quartz solubility at low temperatures. Geochim. Cosmochim. Acta 61, 2553–2558.

Rimstidt, J.D., Barnes, H.L., 1980. The kinetics of silica–water reactions. Geochim. Cosmochim. Acta 44, 1683–1699.

Rosanski, K., Araguás-Araguás, L., 1995. Spatial and temporal variability of stable isotope composition of precipitation over the South American continent. Bull. Inst. Francais Études Andines 24 (3), 379–390.

Rosenthal, E., Jones, B.F., Weinberger, G., 1998. The chemical evolution of Kurnub Group paleowater in Sinai-Negev province – a mass balance approach. Appl. Geochem. 13 (5), 553–569.

Shinzato, M.C., Montanheiro, T.J., Janasi, V.A., Negri, F.A., Yamamoto, J.K., Andrade, S., 2008. Caracterização tecnológica das zeólitas naturais associadas às rochas eruptivas da Formação Serra Geral, na região de Piraju-Ourinhos (SP). Revista Brasileira de Geociências 38 (3), 525–532.

da Silva, R.B.G., 1983. Estudo Hidroquímico e isotópico do Aquífero Botucatu no Estado de São Paulo. Tese (Doutorado em Geologia). Instituto de Geociências, Universidade de São Paulo, São Paulo, 133p.

Sracek, O., Hirata, R., 2002. Geochemical and stable isotopic evolution of the guarani aquifer in the State of São Paulo, Brazil. Hydrogeol. J. 10, 643–655.

Vuille, M., Werner, M., 2005. Stable isotopes in precipitation recording South American summer monsoon and ENSO variability: observations and model results. Climate Dyn. 25, 401–413.

Vuille, M., Bradley, R.S., Werner, M., Healy, R., Keimig, F., 2003. Modeling $\delta^{18}O$ in precipitation over the tropical Americas: 1. Interannual variability and climatic controls. J. Geophys. Res. 108, 4174.

Wahnfried, I., 2010. Modelo Conceitual de Fluxo do Aquitarde Serra Geral e do Sistema Aquífero Guarani na Região de Ribeirão Preto (SP). Tese (Doutorado em Geologia). Instituto de Geociências, Universidade de São Paulo, São Paulo, 124p.